PCCP

ROYAL SOCIETY OF CHEMISTRY

PAPER

Cite this: *Phys. Chem. Chem. Phys.*, 2023, **25**, 29257

Confinement-induced nonlocality and casimir force in transdimensional systems

Igor V. Bondarev, *[a] Michael D. Pugh, [a] Pablo Rodriguez-Lopez, [bc] Lilia M. Woods [d] and Mauro Antezza [ce]

Received 2nd August 2023,
Accepted 2nd October 2023

DOI: 10.1039/d3cp03706a

rsc.li/pccp

We study within the framework of the Lifshitz theory the long-range Casimir force for in-plane isotropic and anisotropic free-standing transdimensional material slabs. In the former case, we show that the confinement-induced nonlocality not only weakens the attraction of ultrathin slabs but also changes the distance dependence of the material-dependent correction to the Casimir force to go as $\sim 1/\sqrt{l}$ contrary to the $\sim 1/l$ dependence of that of the local Lifshitz force. In the latter case, we use closely packed array of parallel aligned single-wall carbon nanotubes in a dielectric layer of finite thickness to demonstrate strong orientational anisotropy and crossover behavior for the inter-slab attractive force in addition to its reduction with decreasing slab thickness. We give physical insight as to why such a pair of ultrathin slabs prefers to stick together in the perpendicularly oriented manner, rather than in the parallel relative orientation as one would customarily expect.

I. Introduction

Modern fabrication techniques have appreciably improved the quality of thin films, making it possible to produce ultrathin films of precisely controlled thickness down to a few monolayers.[1–10] Such ultrathin films, often referred to as transdimensional (TD) quantum materials or TD metasurfaces (MSs),[10–12] offer high tailorability of their electronic and optical properties not only by altering their chemical and electronic composition (stoichiometry, doping) but also by varying their thickness (the number of monolayers).[13–24] Whereas three-dimensional (3D) bulk materials allow for higher free carrier concentration, and their two-dimensional (2D) counterparts such as graphene and monolayer transition metal dichalcogenides provide the strong confinement of exciton–polariton and plasmon modes,[25–27] the advantages of both of these extremes can be merged by using TD quantum systems.[11] For such systems, quite generally, the vertical quantum confinement leads to an effective dimensionality reduction from 3D to 2D while still retaining the thickness as a parameter to represent the vertical size.[28–30]

Since the TD regime is situated in-between the 3D and 2D dimensionalities, quantum-confined TD materials make it possible to probe fundamental properties of light–matter interactions as they evolve from a single atomic layer to a larger number of layers approaching the bulk material properties.[14,19] Ultrathin films of metals, doped semiconductors or polar materials with thickness of only a few monolayers can support plasmon, exciton and phonon–polariton modes.[3–10] Due to their localized plasmon modes[20,24] and associated thickness-dependent photonic density of states,[13,19] they can provide controlled light confinement and tunable light–matter coupling which makes them distinctly different from conventional thin films. Fundamental properties of the TD systems originate from the quantum-confined electromagnetic (EM) dispersion of their eigen excitation modes and cannot be inferred from those of 2D systems or 3D materials with boundary conditions imposed on their top and bottom interfaces.[19] Vertical confinement makes these modes nonlocal and so distinct from those of conventional thin films. Confinement-induced nonlocality is the remarkable intrinsic property of the in-plane EM response of TD systems.[24] It is this nonlocality that enables a variety of new quantum phenomena in ultrathin films, including thickness-controlled plasma frequency red shift,[10,31] low-temperature plasma frequency dropoff,[32] plasmon mode degeneracy lifting and spontaneous emission enhancement,[19] directional negative refractivity,[17] absorption-transmission switching under controlled exciton–plasmon coupling,[18] a series of quantum-optical,[14] magneto-optical[22] and radiative heat transfer effects[33,34] as well as quantum electronic transitions that are normally forbidden.[35]

[a] *Department of Mathematics & Physics, North Carolina Central University, Durham, NC 27707, USA. E-mail: ibondarev@nccu.edu*
[b] *Área de Electromagnetismo and Grupo Interdisciplinar de Sistemas Complejos (GISC), Universidad Rey Juan Carlos, 28933 Móstoles, Madrid, Spain*
[c] *Laboratoire Charles Coulomb (L2C), UMR 5221 CNRS-University of Montpellier, F-34095 Montpellier, France*
[d] *Department of Physics, University of South Florida, Tampa, FL 33620, USA*
[e] *Institut Universitaire de France, 1 rue Descartes, F-75231 Paris Cedex 05, France*

The confinement-induced nonlocal EM response comes from the Keldysh–Rytova (KR) pairwise interaction potential.[20,24] The KR interaction potential takes into account the vertical electron (and/or hole) confinement due to the presence of substrate and superstrate with dielectric permittivities much less (*e.g.*, air) than the in-plane dielectric permittivity of the film itself.[28,29] For ultrathin films such a potential is much stronger than the Coulomb interaction potential. It transitions into the electrostatic Coulomb potential with film thickness increase, which is why the thickness can be treated as a parameter to control the optical response of TD films. The nonlocal KR model of the EM response is unique in that it covers the entire range from atomically thin to conventional films of the order of a few optical wavelengths in thickness.[10,19] Previously,[33] a comparative analysis of the nonlocal and standard local (Drude) EM response models reported significant differences in their predictions of far- and near-field heat transfer properties of the TD film systems. Very recently, the nonlocal EM response model was successfully tested experimentally.[34] It is this nonlocal model that we use here for theoretical studies into a closely related phenomenon – the Casimir effect in ultrathin TD systems. The Lifshitz theory we employ herein,[36,37] conveniently represents molecular attractive forces between solids in terms of their respective linear EM response functions. We calculate the long-range attractive force between two free-standing ultrathin TD material slabs as functions of their thickness and separation distance. The geometries considered are shown in Fig. 1, where (a) is the case of two identical in-plane isotropic slabs, while (b) and (c) sketch the two relative orientations for in-plane anisotropic finite-thickness slabs made of densely-packed parallel-aligned periodic single-wall carbon nanotube (SWCN) arrays studied recently in ref. 17. We show that the confinement-induced nonlocality of the EM response leads to significant reduction of the attractive force. In the in-plane anisotropic case, additionally, we predict strong orientational anisotropy and crossover behavior for the attractive force in the (b) and (c) orientations depending on the film thickness and SWCN diameter variation. The following sections describe our model, present our theoretical results, and conclude our work by summarizing its key findings.

II. Casimir effect for a pair of parallel TD material slabs

We start with the long-range attractive force expression of the Lifshitz theory for molecular attractive forces between solids at zero temperature.[36,37] In this case the separation distance between the slabs sketched in Fig. 1 is larger than the fundamental wavelength of their absorption spectra, whereby the force takes the following form[36]

$$F = \frac{\hbar c}{32\pi^2 l^4}\int_0^\infty \mathrm{d}x \int_1^\infty \mathrm{d}p\, \frac{x^3}{p^2}\left\{\left[\frac{(s_1+p)(s_2+p)}{(s_1-p)(s_2-p)}\, e^x - 1\right]^{-1} + \left[\frac{(s_1+\varepsilon_1 p)(s_2+\varepsilon_1 p)}{(s_1-\varepsilon_1 p)(s_2-\varepsilon_1 p)}\, e^x - 1\right]^{-1}\right\}, \quad (1)$$

$$\varepsilon_{1,2} = \varepsilon_{1,2}\left(i\frac{xc}{2pl}\right),\ s_{1,2} = \sqrt{\varepsilon_{1,2}\left(i\frac{xc}{2pl}\right) - 1 + p^2}.$$

Here, c is the speed of light, l is the distance between the slabs of an infinitely large in-plane size, and $\varepsilon_{1,2}(\omega)$ are their respective linear EM response functions (dynamical dielectric permittivities) treated as functions of the complex variable $\omega = i\xi$ with $\xi = xc/(2pl)$.

For a pair of perfectly conducting metallic plates, in which case $\varepsilon_{1,2} = \infty$, eqn (1) can be integrated exactly to give the well known Casimir force[38]

$$F_C = \frac{\hbar c}{l^4}\frac{\pi^2}{240}. \quad (2)$$

In terms of the Lifshitz theory, however, the Casimir force is just the zero-order expansion term of eqn (1). The next expansion term can be obtained if one uses the explicit form of the dynamical dielectric functions $\varepsilon_{1,2}(\omega)$ in the frequency range that contributes the most to the integral in eqn (1). It can be

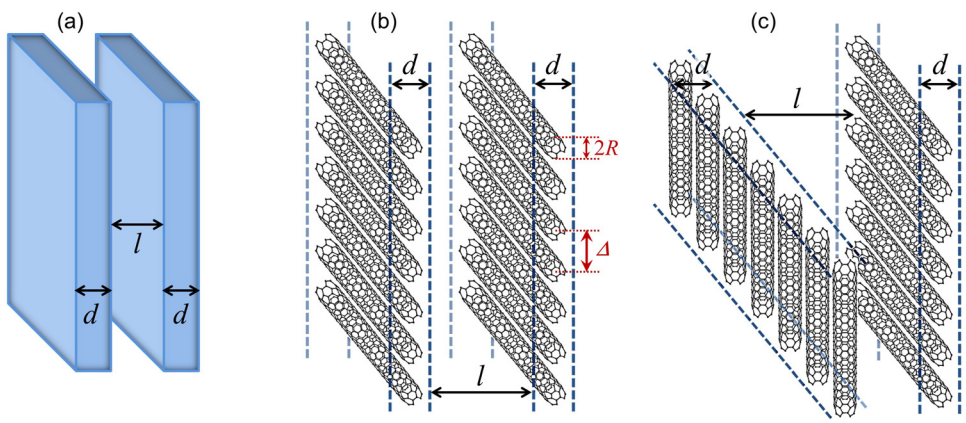

Fig. 1 Finite-thickness parallel material slabs studied in this work. (a) Two identical in-plane isotropic slabs. (b) and (c) Two relative orientations for in-plane anisotropic slabs made of parallel-aligned periodic SWCN arrays. Monolayers shown are just for a sketch. The actual slabs we study are composed of a varied number of densely-packed monolayers. See text for details.

seen that this is the domain where $p \sim 1$ and $x \sim 1$, or $\omega/c \sim 1/l \sim 0$ since $x = 2pl\xi/c$ and $\omega = i\xi$ as per the Lifshitz theory in the large separation limit.[36] For normal metals commonly described by the standard low-frequency local (Drude) EM response function

$$\varepsilon(\omega) = \varepsilon_b - \frac{{\omega_p}^2}{\omega(\omega + i\delta)}, \tag{3}$$

where ε_b is the constant background permittivity, δ stands for the damping constant,

$$\omega_p = \omega_p^{3D} = \sqrt{\frac{4\pi e^2 N_{3D}}{m^*}}, \tag{4}$$

ω_p^{3D} is the bulk plasma frequency, and other parameters have their usual meanings, the Casimir force in eqn (2) comes out of the Lifshitz theory as the main (zero-order) power series expansion term of the function $\varepsilon(\omega)$ at infinity in the integrand of eqn (1). This term can be obtained by using the $\varepsilon(\omega \to 0) = -\infty$ limit in eqn (1). The correction to it comes from the next series expansion term of the function $\varepsilon(\omega)$ at infinity in the integrand of eqn (1). This is totally contributed by the addend of eqn (3), $\Delta\varepsilon = -{\omega_p}^2/\omega^2$ (damping neglected for simplicity), in the first nonvanishing order of the integrand power series expansion in eqn (1) under the condition $1/\sqrt{\Delta\varepsilon_{1,2}} \ll p \ll \sqrt{\Delta\varepsilon_{1,2}}$. For identical metals this gives[36]

$$F_L = F_C\left(1 - \frac{16c}{3\omega_p l}\right) \tag{5}$$

referred to as the Lifshitz force in what follows, where the second term in parentheses is the legitimate correction to the first at separations greater than that at which they are comparable. This term cannot be derived by the method of ref. 38 where the main term (2) was first obtained.

A. In-plane isotropic TD systems

For in-plane isotropic TD material films, due to the KR pairwise interaction potential of the charge carriers in it, the in-plane plasma oscillation frequency is given by the nonlocal expression as follows[24]

$$\omega_p(k) = \frac{\omega_p^{3D}}{\sqrt{1 + 1/(\tilde{\varepsilon}kd)}}. \tag{6}$$

Here, $\tilde{\varepsilon} = \varepsilon_b/(\varepsilon_1 + \varepsilon_2)$ with $\varepsilon_{1,2}$ ($< \varepsilon_b$) being the film substrate and superstrate static permittivities, ε_b is the in-plane dielectric permittivity of the film (contributed by both positive ion background and interband electronic transitions), d is its thickness, and k is the in-plane electron momentum absolute value. The low-energy in-plane EM response function of the film is still given by eqn (3), but now with ω_p replaced by that of eqn (6), which makes the in-plane dielectric response function k-dependent and so spatially dispersive, or nonlocal. This is the essence of the nonlocal EM response model for TD quantum materials.[19,33] With d decreasing, it can be seen that $\omega_p(k)$ shifts to the red and eqn (6) acquires the $\sqrt{k}$-type nonlocal spatial dispersion of 2D materials. As d increases and becomes sufficiently large, eqn (6) can be seen to gradually approach ω_p^{3D}, the bulk material screened plasma frequency (4), and the EM response function (3) takes the standard local Drude form.

The procedure described above to obtain the Lifshitz force (5) can be repeated for a pair of identical in-plane isotropic TD material slabs, sketched in Fig. 1(a), using the nonlocal EM response function of the slabs as given by eqn (3) and (6). After having done the above mentioned substitution of variables and having also used the equality $\omega p/c = \sqrt{(\omega/c)^2 - k^2}$ for the in-plane momentum k to fulfill,[36,37] eqn (1) can be simplified to give the thickness dependent expression as follows

$$F = F_C\left[1 - \frac{15c}{\pi^4\omega_p^{3D}l}\int_0^\infty dx\,\frac{x^4e^x}{(e^x-1)^2} \times \int_1^\infty dp\,\frac{p^2+1}{p^4}\sqrt{1 + \frac{2l}{\tilde{\varepsilon}d}\,\frac{p}{x\sqrt{p^2-1}}}\right]. \tag{7}$$

In this equation the square root can be seen to tend to unity as $d \to \infty$. The remaining integral can be done analytically to give the Lifshitz force (5). In the opposite limit where d becomes sufficiently small (see Section IIIC for more precise definition of this term), one has

$$\begin{aligned} F &= F_C\left[1 - \frac{15\sqrt{2}c}{\pi^4\omega_p^{3D}\sqrt{\tilde{\varepsilon}dl}}\int_0^\infty dx\,\frac{x^{7/2}e^x}{(e^x-1)^2}\int_1^\infty dp\,\frac{p^2+1}{p^{7/2}\sqrt[4]{p^2-1}}\right] \\ &= F_C\left(1 - \frac{4.79c}{\omega_p^{3D}\sqrt{\tilde{\varepsilon}dl}}\right). \end{aligned} \tag{8}$$

Here, the correction term in parentheses goes with inter-slab separation distance as $1/\sqrt{l}$, much slower than the $1/l$ dependence of the correction term in the Lifshitz force (5). The ratio of the former over the latter can be approximated as $\sqrt{l/(\tilde{\varepsilon}d)} > 3$ for all $l > 0.5$ μm with $d = 10$ nm and $\tilde{\varepsilon} = 4.5$ (parameters chosen as discussed in Section III), indicating that the attraction force is weaker due to the confinement-induced EM response nonlocality and can also be controlled by material optical properties and thickness.

B. In-plane anisotropic TD systems

As an example of an in-plane anisotropic TD system we focus on a closely packed array of periodically aligned SWCNs of radius R, with translational unit Δ, embedded in a dielectric layer of thickness d as shown in Fig. 1(b) and (c). Material systems like that are currently in the process of intensive experimental development,[39–41] with a great potential to become the next generation advanced flexible platform for multifunctional metasurfaces and nonlinear optical devices with adjustable characteristics on demand.[42–49]

Collective EM response of a TD material slab made of periodically aligned SWCN arrays was recently studied theoretically.[17,20] Being contributed by both plasmons and excitons (corresponding to intra- and interband transitions in the infrared and optical spectral regions, respectively), it was shown to be strongly anisotropically nonlocal due to the

cylindrical spatial anisotropy, periodic in-plane transverse inhomogeneity, and vertical quantum confinement of the system. In the direction perpendicular to the SWCN alignment the in-plane response is a constant dielectric permittivity ε_b effectively. In the SWCN alignment direction it is the complex-valued momentum-dependent (nonlocal) dynamical function given by eqn (3) in the low-energy region of interest here,[17] but now with[20]

$$\omega_p(q) = \omega_p^{3D}\sqrt{\frac{2qRI_0(qR)K_0(qR)}{1+1/(q\tilde{\varepsilon}d)}} \tag{9}$$

representing the intraband plasma oscillation frequency for a finite-thickness, cylindrically anisotropic, periodically aligned (metallic or semiconducting) SWCN array. Here, ω_p^{3D} is given by eqn (4) with $N_{3D} = N_{2D}/d$, q stands for the absolute value of the electron momentum along the SWCN alignment direction and makes the EM response of the slab unidirectionally nonlocal, I_0 and K_0 are the zeroth-order modified cylindrical Bessel functions responsible for the correct normalization of the electron density distribution over cylindrical surfaces, to give for $R \to \infty$, whereby $qRI_0(qR)K_0(qR) \to 1/2$, the isotropic TD film plasma frequency of eqn (6) studied previously in ref. 19 and 33 and tested experimentally for TiN films of varied thickness both at room[10] and at cryogenic temperatures.[32] This EM response function features no bandstructure of individual SWCNs as it is contributed by intraband transitions alone, in which case their intrinsic properties are only determined by the carbon–carbon overlap integral (accounted for in N_{2D}) and by the surface curvature represented by R here.

By symmetry, there are two minimum-energy relative orientations possible for a pair of identical space-separated finite-thickness SWCN slabs. They are shown in Fig. 1(b) and (c). Their respective attractive forces $F_\parallel$ and $F_\perp$ can be obtained from the Lifshitz formula of eqn (1) by noticing that the two terms under the integral sign there represent the inter-slab virtual s- and p-polarized photon exchange, respectively. Since (i) we only have one direction for plasmon propagation on each of the slabs – the one defined by q-vector of eqn (9) which is along the SWCN alignment direction, (ii) plasmons can only be excited by p-polarized photons, and (iii) each of the slabs is a dielectric in the direction perpendicular to the SWCN alignment direction, the two attractive forces in (b) and (c) orientations of identical slabs in Fig. 1 come out of eqn (1) in the form as follows

$$F_\parallel = \frac{\hbar c}{32\pi^2 l^4}\int_0^\infty \mathrm{d}x \int_1^\infty \mathrm{d}p \frac{x^3}{p^2}\left\{\left(\varphi^2 e^x - 1\right)^{-1} + \left[\left(\frac{s+\varepsilon p}{s-\varepsilon p}\right)^2 e^x - 1\right]^{-1}\right\},$$

$$F_\perp = \frac{\hbar c}{32\pi^2 l^4}\int_0^\infty \mathrm{d}x \int_1^\infty \mathrm{d}p \frac{x^3}{p^2}\left[\left(\varphi\frac{s+p}{s-p}e^x - 1\right)^{-1} + \left(\psi\frac{s+\varepsilon p}{s-\varepsilon p}e^x - 1\right)^{-1}\right], \tag{10}$$

$$\varepsilon = \varepsilon\left(i\frac{xc}{2pl}\right),\ s = \sqrt{\varepsilon\left(i\frac{xc}{2pl}\right) - 1 + p^2},$$

$$\varphi = \frac{\sqrt{\varepsilon_b - 1 + p^2} + p}{\sqrt{\varepsilon_b - 1 + p^2} - p},\ \psi = \frac{\sqrt{\varepsilon_b - 1 + p^2} + \varepsilon_b p}{\sqrt{\varepsilon_b - 1 + p^2} - \varepsilon_b p}.$$

Here, ε is given by eqn (3) with plasma frequency of eqn (9) and the functions φ and ψ represent the metallic-type EM response in the SWCN alignment direction and the dielectric background response in the in-plane perpendicular direction, respectively.

Now the procedure described above to derive eqn (7) can be repeated for $F_\parallel$ and $F_\perp$ of eqn (10) separately. This results in the attractive force expressions representative of the SWCN array with parameters R, Δ and slab thickness d, as follows

$$F_\parallel = F_C\left[\frac{1}{2} + \frac{15}{2\pi^4}\int_0^\infty \mathrm{d}x \int_1^\infty \mathrm{d}p \frac{x^3}{p^2}\frac{1}{\varphi^2 e^x - 1} - \frac{15c}{\pi^4\omega_p^{3D} l}\int_0^\infty \mathrm{d}x \int_1^\infty \mathrm{d}p \frac{x^4}{p^4}\frac{e^x}{(e^x-1)^2}\sqrt{\frac{\Delta}{4\pi R}\frac{\alpha(1+R\alpha/\tilde{\varepsilon}d)}{I_0(1/\alpha)K_0(1/\alpha)}}\right] \tag{11}$$

with $\alpha = \dfrac{2l}{R}\dfrac{p}{x\sqrt{p^2-1}}$ and

$$F_\perp = F_C\left\{\frac{15}{2\pi^4}\int_0^\infty \mathrm{d}x \int_1^\infty \mathrm{d}p \frac{x^3}{p^2}\left(\frac{1}{\varphi e^x - 1} - \frac{1}{\psi e^x + 1}\right) - \frac{15c}{2\pi^4\omega_p^{3D} l}\int_0^\infty \mathrm{d}x \int_1^\infty \mathrm{d}p \frac{x^4 e^x}{p^3}\left[\frac{\varphi p}{(\varphi e^x - 1)^2} - \frac{\psi/p}{(\psi e^x + 1)^2}\right] \times \sqrt{\frac{\Delta}{4\pi R}\frac{\alpha(1+R\alpha/\tilde{\varepsilon}d)}{I_0(1/\alpha)K_0(1/\alpha)}}\right\}. \tag{12}$$

Taking the limit $\omega_p^{3D} \to +\infty$ in these equations is the same as taking the limit $\omega \to 0$ in eqn (3). This leaves us with the main expansion term alone in both equations, of which that in eqn (12) reproduces the metal–dielectric attractive force first reported by Lifshitz in his seminal work.[36] Both terms are shown in Fig. 2 as functions of $1/\varepsilon_b$ relative to F_C, the Casimir force, to demonstrate the role of the dielectric background in the orientational anisotropy of the attractive force in our system. The anisotropy increases with decreasing ε_b as expected due to the relative increase of the unidirectional metallic-type

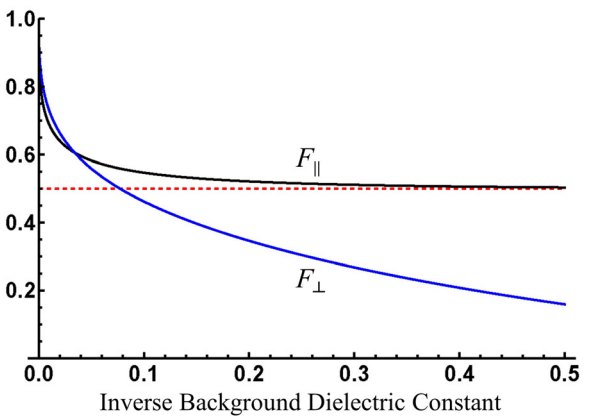

Fig. 2 Orientational anisotropy of the attractive force for free-standing slabs sketched in Fig. 1(b) and (c), relative to the Casimir force.

EM response component. Both terms become equal to F_C in the limit $\varepsilon_b \to \infty$, an analogue of the perfect metal case.

III. Numerical results and discussion

For all three cases of space-separated finite-thickness slabs shown in Fig. 1(a)–(c), the bulk plasma frequency is the main parameter of the long-range nonlocal attractive force in eqn (7), (11) and (12) we have obtained. We use a typical free-electron-gas value $\omega_p^{3D} = 2 \times 10^{16}\ s^{-1}$ estimated from $N_{3D} \approx 10^{23}\ cm^{-3}$ in our calculations we discuss below.

A. In-plane isotropic TD systems

Fig. 3 shows our numerical results for the nonlocal attraction force obtained from eqn (7) for the free-standing slabs of varied thickness. The background in-plane dielectric permittivity constant $\varepsilon_b = 9$ was used in these calculations, which is close to those reported experimentally for typical ultrathin plasmonic films.[10,33] Fig. 3(a) compares the force calculated for the three slab thicknesses, $d = 10$ nm, 20 nm and 200 nm (black, blue and green line, respectively), to the Lifshitz force of eqn (5) and to the Casimir force for perfect metals of eqn (2). It can be seen that the confinement-induced nonlocality weakens significantly the attraction of the thinner slabs. Increasing of the slab thickness diminishes this effect, making the force approach the local Lifshitz limit, which in itself is significantly less than the Casimir force at shorter inter-slab distances. This can also be seen in Fig. 3(b), which shows the nonlocal attraction force together with the Lifshitz force relative to the Casimir force as functions of slab thickness and inter-slab distance. Contrary to the Lifshitz force, the nonlocal attraction force can now be seen to quickly drop down with decreasing slab thickness, approaching the form in eqn (8) where the nonlocal correction term is $\sim 1/\sqrt{l}$ as opposed to the $1/l$ dependence of the local Lifshitz force in eqn (5).

B. In-plane anisotropic TD systems

Fig. 4 summarizes our numerical data obtained for the slab thickness and inter-slab distance dependences of the anisotropic nonlocal attraction forces $F_\parallel$ and $F_\perp$ (relative to the Casimir force) as given by eqn (11) and (12) for densely packed ($\Delta = 2R$) free-standing SWCN arrays oriented as shown in Fig. 1(b) and (c), respectively. In (a), the forces are shown for the five-monolayer-thick slabs composed of SWCNs of increasing radius. In (b), they are shown for the slabs composed of the 2 nm-radius SWCN array monolayer of increasing monolayer number. In both cases the slab thickness increases either due to the SWCN radius with monolayer number fixed, or due to the monolayer number with SWCN radius fixed. Lightly colored planes on top show the main expansion terms of eqn (11) and (12) one obtains in the limit $\omega_p^{3D} \to +\infty$, or $\omega \to 0$ in eqn (3), whereby the SWCN array structural parameters disappear and the dielectric background constant ε_b remains the only parameter to control the difference between $F_{||}$ and $F_\perp$ as discussed for Fig. 2. Both (a) and (b) show the graphs calculated for $\varepsilon_b = 10$ (*cf.* Fig. 2). In (c) and (d) the same is shown for $\varepsilon_b = 5$.

In addition to the reduction of the attractive force with decreasing slab thickness we have seen above for the in-plane isotropic case, there is one more remarkable non-obvious feature that can now be seen in Fig. 4. This is the crossover behavior of the attractive force: namely, the force $F_{||}$, which is always greater than $F_\perp$ for thicker slabs, weakens quickly with slab thickness reduction and becomes less than the force $F_\perp$ for sufficiently thin slabs. This means that a pair of ultrathin slabs prefers to stick together in the perpendicularly oriented manner sketched in Fig. 1(c), counter-intuitively, rather than in the parallel relative orientation shown in Fig. 1(b) one would think of customarily. Although not obvious at first glance, this crossover behavior can still be understood as being due to the increased transmission of the metallic-type EM response component in our system, facilitated by the plasma frequency red shift as the slab thickness d in eqn (9) decreases. Metals are known to be transmissive in the frequency range above their plasma frequency (see, *e.g.*, ref. 50), which now shifts towards infrared. Increased metallic transmission reduces photon absorption necessary for inter-slab attraction to occur.[36,37] Hence, it follows from eqn (10) that a pair of parallel oriented slabs with metal–metal/dielectric–dielectric type of virtual

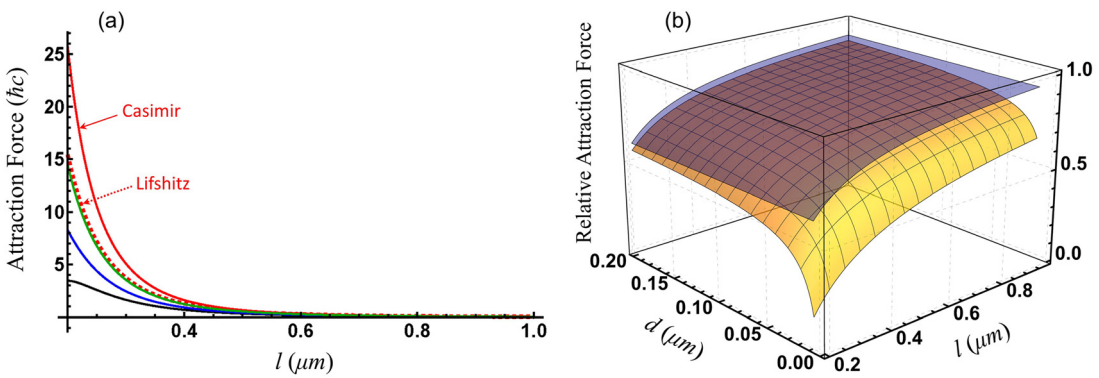

Fig. 3 (a) Nonlocal attraction force for a pair of free-standing in-plane isotropic slabs of 10 nm (black), 20 nm (blue) and 200 nm (green) in thickness, as given by eqn (7). Short-dashed red line is the Lifshitz force of eqn (5). (b) Lifshitz force (dark blue) and nonlocal attraction force (yellow) as functions of the slab thickness and inter-slab distance, relative to the Casimir force.

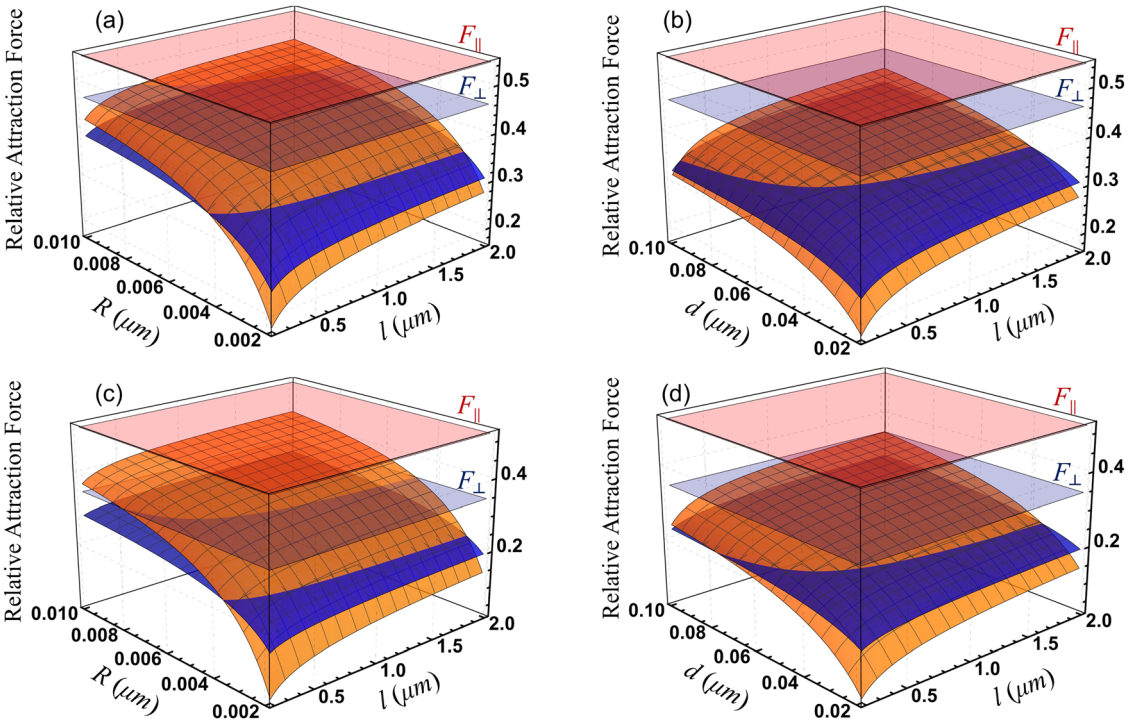

Fig. 4 Anisotropic nonlocal attraction forces $F_\parallel$ and $F_\perp$ as functions of the slab thickness and inter-slab distance, relative to the Casimir force. (a) 5-monolayer-thick free-standing slabs composed of SWCNs of increasing radius and (b) slabs of increasing thickness composed of 2 nm-radius SWCNs, as given by eqn (11) and (12) with $\varepsilon_b = 10$. In (c) and (d) same is shown for $\varepsilon_b = 5$. Lightly colored planes on top show the main expansion terms given by eqn (11) and (12) in the limit $\omega_p^{3D} \to +\infty$, or $\omega \to 0$ in eqn (3), whereby the SWCN array structural parameters are gone.

photon exchange becomes less attractive than a pair of perpendicularly oriented slabs with metal–dielectric/dielectric–metal type of virtual photon exchange as the former is associated with twice less absorption (roughly) than the latter. Decreasing of the dielectric background constant ε_b leads to the relative weight increase for the metallic type EM response, just like it would be a pair of thicker slabs, which is why the crossover effect in (c) and (d) can be seen to shift toward smaller slab thicknesses as compared to those in (a) and (b).

C. Can the Lifshitz formula be applied to ultrathin films?

The Lifshitz formula we use herein was originally obtained for two media filling space-separated half-spaces with plane-parallel boundaries.[36] In practice, however, one always deals with finite-thickness material slabs. Hence, there are two questions we should answer to justify the Lifshitz formula applicability in our case: (i) is it appropriate to replace bulk material EM response functions of the Lifshitz model by their thickness dependent in-plane counterparts we use, and (ii) what is the smallest thickness for a material slab to correctly represent medium-filled half-space. Both questions are addressed in what follows.

For question (i), we note that to obtain the attraction force between the two space-separated material half-spaces as a function of their out-of-plane separation distance alone, one necessarily has to integrate over the two in-plane directions. This is what the Lifshitz model does assuming (customarily) the bulk-medium linear EM response to be the same in all three directions, of which two in-plane directions are integrated over while the out-of-plane one remains to represent the distance dependence of interest. This is equivalent to using the thickness-dependent in-plane EM response functions in the integration directions we do here, whereby the Lifshitz model consistency is preserved.

In order to answer question (ii), it is sufficient to compare the s and p wave reflection coefficients $r_{s,p}$ given by the reciprocals of the pre-exponential factors in the first and second terms of eqn (1), respectively, with those of the free-standing film of thickness d (see, *e.g.*, ref. 19 and 33)

$$R_{s,p} = \frac{r_{s,p}\left[1 - e^{2id\sqrt{\varepsilon(k,\omega)(\omega/c)^2 - k^2}}\right]}{1 - r_{s,p}^2 e^{2id\sqrt{\varepsilon(k,\omega)(\omega/c)^2 - k^2}}}$$

after the required substitutions of variables $\omega p/c = \sqrt{(\omega/c)^2 - k^2}$, $\omega = ixc/(2pl)$ are done. Here, the exponential factor is responsible for the backscattering from the second interface that is now present in the system. Using eqn (3) with damping neglected as before, we have

$$2id\sqrt{\varepsilon(k,\omega)\frac{\omega^2}{c^2} - k^2} = -2d\frac{\omega_p^{3D}}{c}\sqrt{1 + \frac{x^2(p^2 + \varepsilon_b - 1)}{p^2}\left(\frac{c}{2l\omega_p^{3D}}\right)^2},$$

where $x \sim 1$ and $p \geq 1$ as it follows from the structure of the integral expression in eqn (1). We also have $c/\omega_p^{3D} = 3 \times 10^8\ \mathrm{m\ s^{-1}}/(2 \times 10^{16}\ \mathrm{s^{-1}}) = 15$ nm, so that $c/(2l\omega_p^{3D}) < 1$ for all $l > 10$ nm and $2d\omega_p^{3D}/c > 1$ for all $d > 10$ nm, whereby the backscattering from

the second interface becomes exponentially suppressed making the coefficients $R_{s,p}$ indistinguishable from $r_{s,p}$ for films greater than 10 nm in thickness. The data we present in Fig. 3 and 4 above never fall out of this range.

IV. Conclusion

In this work, we use the Lifshitz theory to explore the impact of the confinement-induced nonlocality of the material EM response on the (Casimir) force of attraction between two space-separated TD material slabs. The Lifshitz theory represents molecular attractive forces between solids in terms of their respective linear EM response functions for which we use those provided by the confinement-induced nonlocal EM response model.[20,24] Confinement-induced is a special type of nonlocality that comes from the KR pairwise electron interaction potential in optically dense ultrathin films of finite thickness.[28,29] This potential is stronger than the Coulomb interaction potential and depends on the film thickness, which is why our EM response model covers both ultrathin ($d \gtrsim 10$ nm) and conventional thin films.[33] In general, the Lindhard-Mermin nonlocality of bulk materials might also play a role for thicker slabs;[51] however, this is the k^2-infinitesimal order nonlocality, which in the most important low-momentum domain is much less than the confinement-induced k-infinitesimal order nonlocality of the KR model we use.[24]

We calculate the long-range attractive forces for in-plane isotropic and anisotropic free-standing TD material slabs. In the former case, we show that the confinement-induced nonlocality not only weakens the attraction of ultrathin slabs but also changes the distance dependence of the material-dependent correction to the Casimir force to go as $\sim 1/\sqrt{l}$ contrary to the $\sim 1/l$ dependence of that of the local Lifshitz force. Increasing the slab thickness diminishes this effect, making the force approach the local Lifshitz force limit which in itself is significantly less than the material-independent Casimir force. In the latter case, we use closely packed array of single-diameter parallel aligned SWCNs in a dielectric layer of finite thickness to demonstrate strong orientational anisotropy and crossover behavior for the inter-slab attractive force in addition to its reduction with decreasing slab thickness. We show that and we explain why a pair of ultrathin slabs prefers to stick together in the perpendicularly oriented manner, rather than in the parallel relative orientation as one would customarily expect and as it is shown to occur for thicker slabs.

Our results are obtained for optically dense closely-packed TD films – films possessing a well-pronounced collective low-frequency EM response (plasmons) – in the long-range low-temperature quantum limit $lk_BT/(\hbar c) \ll 1$ of the Lifshitz theory.[36] For $l \lesssim 1$ μm where the effects we discuss occur, this becomes $T \ll 2000$ K so that high-temperature calculations in the classical limit will hardly affect our reported results. Another case is that of diluted quasi-2D films, where the electron band-structure and many-body EM exchange interactions are predominantly controlled by dimensionality and by restricted geometry,[52–55] and so temperature effects,[52] many-body retardation effects[53–55] as well as purely quantum effects such as electron energy-level quantization and wavefunction spill-out,[56] which are not involved in our case, can be important.

Conflicts of interest

The authors declare no conflicts of interest.

Acknowledgements

I. V. B. is supported by the U.S. Army Research Office under award No. W911NF2310206. M. D. P. was supported by the U.S. National Science Foundation grant No. DMR-1830874 (awarded to I.V.B.). P. R.-L. acknowledges support from AYUDA PUENTE 2022, URJC and QuantUM program of the University of Montpellier. P. R.-L. would like to thank the University of Montpellier and the theory group for Light-Matter and Quantum Phenomena of the Laboratoire Charles Coulomb for hospitality during his stay in Montpellier where part of this work was done. L. M. W. acknowledges financial support from the US Department of Energy under Grant No. DE-FG02-06ER46297. M. A. acknowledges the grant ''CAT'', No. A-HKUST604/20, from the ANR/RGC Joint Research Scheme sponsored by the French National Research Agency (ANR) and the Research Grants Council (RGC) of the Hong Kong Special Administrative Region. I. V. B., L. M. W. and M. A. gratefully acknowledge support from the Kavli Institute for Theoretical Physics (KITP), UC Santa Barbara, under U.S. National Science Foundation Grant No. PHY-1748958, where this collaborative work was started. I. V. B. acknowledges KITP hospitality during his invited visit as a KITP Fellow 2022–23 made possible by the Heising-Simons Foundation.

References

1 A. Kossoy, V. Merk, D. Simakov, K. Leosson, S. Kéna-Cohen and S. A. Maier, Optical and structural properties of ultrathin gold films, *Adv. Opt. Mater.*, 2015, **3**, 71.
2 D. Shah, H. Reddy, N. Kinsey, V. M. Shalaev and A. Boltasseva, Optical properties of plasmonic ultrathin TiN films, *Adv. Opt. Mater.*, 2017, **5**, 1700065.
3 D. Shah, A. Catellani, H. Reddy, N. Kinsey, V. M. Shalaev, A. Boltasseva and A. Calzolari, Controlling the plasmonic properties of ultrathin TiN films at the atomic level, *ACS Photonics*, 2018, **5**, 2816.
4 A. M. Dubrovkin, B. Qiang, H. N. S. Krishnamoorthy, N. I. Zheludev and Q. J. Wang, Ultra-confined surface phonon polaritons in molecular layers of van der Waals dielectrics, *Nat. Commun.*, 2018, **9**, 1762.
5 A. Rodríguez Echarri, J. D. Cox and F. J. García de Abajo, Quantum effects in the acoustic plasmons of atomically thin heterostructures, *Optica*, 2019, **6**, 630.

6 Z. M. Abd El-Fattah, V. Mkhitaryan, J. Brede, L. Fernández, C. Li, Q. Guo, A. Ghosh, A. Rodríguez Echarri, D. Naveh, F. Xia, J. Enrique Ortega and F. J. García de Abajo, Plasmonics in atomically thin crystalline silver films, *ACS Nano*, 2019, **13**, 7771.

7 K. P. Kelley, T. G. Folland, J. Ryan Nolen, N. Engheta, J. D. Caldwell and J.-P. Maria, Polaritonic hybrid-epsilon-near-zero modes: Beating the plasmonic confinement vs propagation-length trade-off with doped cadmium oxide bilayers, *Nano Lett.*, 2019, **19**, 948.

8 R. A. Maniyara, D. Rodrigo, R. Yu, J. Canet-Ferrer, D. S. Ghosh, R. Yongsunthon, D. E. Baker, A. Rezikyan, F. J. García de Abajo and V. Pruneri, Tunable plasmons in ultrathin metal films, *Nat. Photonics*, 2019, **13**, 328.

9 Z. Sun, J. Beaumariage, Q. Wan, H. Alnatah, N. Hougland, J. Chisholm, Q. Cao, K. Watanabe, T. Taniguchi, B. M. Hunt, I. V. Bondarev and D. Snoke, Charged bosons made of fermions in bilayer structures with strong metallic screening, *Nano Lett.*, 2021, **21**, 7669.

10 D. Shah, M. Yang, Z. Kudyshev, X. Xu, V. M. Shalaev, I. V. Bondarev and A. Boltasseva, Thickness-dependent Drude plasma frequency in transdimensional plasmonic TiN, *Nano Lett.*, 2022, **22**, 4622.

11 A. Boltasseva and V. M. Shalaev, Transdimensional photonics, *Nat. Photonics*, 2019, **6**, 1.

12 D. Shah, Z. Kudyshev, S. Saha, V. M. Shalaev and A. Boltasseva, Transdimensional material platforms for tunable metasurface design, *MRS Bull.*, 2020, **45**, 188.

13 L. Zundel, P. Gieri, S. Sanders and A. Manjavacas, Comparative analysis of the near- and far-field optical response of thin plasmonic nanostructures, *Adv. Opt. Mater.*, 2022, **10**, 2102550.

14 I. V. Bondarev, Controlling single-photon emission with ultrathin transdimensional plasmonic films, *Ann. Phys.*, 2023, **535**, 2200331.

15 I. V. Bondarev, O. L. Berman, R. Y. Kezerashvili and Y. E. Lozovik, Crystal phases of charged interlayer excitons in van der Waals heterostructures, *Commun. Phys.*, 2021, **4**, 134.

16 J. Pelliciari, S. Lee, K. Gilmore, J. Li, Y. Gu, A. Barbour, I. Jarrige, C. H. Ahn, F. J. Walker and V. Bisogni, Tuning spin excitations in magnetic films by confinement, *Nat. Mater.*, 2021, **20**, 188.

17 I. V. Bondarev and C. M. Adhikari, Collective excitations and optical response of ultrathin carbon-nanotube films, *Phys. Rev. Appl.*, 2021, **15**, 034001.

18 C. M. Adhikari and I. V. Bondarev, Controlled exciton-plasmon coupling in a mixture of ultrathin periodically aligned single-wall carbon nanotube arrays, *J. Appl. Phys.*, 2021, **129**, 015301.

19 I. V. Bondarev, H. Mousavi and V. M. Shalaev, Transdimensional epsilon-near-zero modes in planar plasmonic nanostructures, *Phys. Rev. Res.*, 2020, **2**, 013070.

20 I. V. Bondarev, Finite-thickness effects in plasmonic films with periodic cylindrical anisotropy [Invited], *Opt. Mater. Express*, 2019, **9**, 285.

21 D. A. Iranzo, S. Nanot, E. J. C. Dias, I. Epstein, C. Peng, D. K. Efetov, M. B. Lundeberg, R. Parret, J. Osmond, J.-Y. Hong, J. Kong, D. R. Englund, N. M. R. Peres and F. H. L. Koppens, Probing the ultimate plasmon confinement limits with a van der Waals heterostructure, *Science*, 2018, **360**, 291.

22 I. V. Bondarev, H. Mousavi and V. M. Shalaev, Optical response of finite-thickness ultrathin plasmonic films, *MRS Commun.*, 2018, **8**, 1092.

23 X. Liu, J.-H. Kang, H. Yuan, J. Park, S. J. Kim, Y. Cui, H. Y. Hwang and M. L. Brongersma, Electrical tuning of a quantum plasmonic resonance, *Nat. Nanotechnol.*, 2017, **12**, 866.

24 I. V. Bondarev and V. M. Shalaev, Universal features of the optical properties of ultrathin plasmonic films, *Opt. Mater. Express*, 2017, **7**, 3731.

25 D. N. Basov, M. M. Fogler, A. Lanzara, F. Wang and Y. Zhang, Colloquium: Graphene spectroscopy, *Rev. Mod. Phys.*, 2014, **86**, 959.

26 K. F. Mak and J. Shan, Photonics and optoelectronics of 2d semiconductor transition metal dichalcogenides, *Nat. Photonics*, 2016, **10**, 216.

27 F. Xia, H. Wang, D. Xiao, M. Dubey and A. Ramasubramaniam, Two-dimensional material nanophotonics, *Nat. Photonics*, 2014, **8**, 899.

28 N. S. Rytova, Screened potential of a point charge in a thin film, *Moscow Univ. Phys. Bull.*, 1967, **3**, 30.

29 L. V. Keldysh, Coulomb interaction in thin semiconductor and semimetal films, *Pis'ma Zh. Eksp. Teor. Fiz.*, 1979, **29**, 716[Engl. translation: JETP Lett. 1980, **29**, 658].

30 M. Kleefstra and G. C. Herman, Influence of the image force on the band gap in semiconductors and insulators, *J. Appl. Phys.*, 1980, **51**, 4923.

31 L. J. Mendoza-Herrera, M. C. Tebaldi, L. B. Scaffardia and D. C. Schinca, Determination of thickness-dependent damping constant and plasma frequency for ultrathin Ag and Au films: Nanoscale dielectric function, *Phys. Chem. Chem. Phys.*, 2022, **24**, 28019.

32 L. Vertchenko, L. Leandro, E. Shkondin, O. Takayama, I. V. Bondarev, N. Akopian and A. V. Lavrinenko, Cryogenic characterization of titanium nitride thin films, *Opt. Mater. Express*, 2019, **9**, 2117.

33 S.-A. Biehs and I. V. Bondarev, Far- and near-field heat transfer in transdimensional plasmonic film systems, *Adv. Opt. Mater.*, 2023, **11**, 2202712.

34 H. Salihoglu, J. Shi, Z. Li, Z. Wang, X. Luo, I. V. Bondarev, S.-A. Biehs and S. Shen, Nonlocal near-field radiative heat transfer by transdimensional plasmonics, *Phys. Rev. Lett.*, 2023, **131**, 086901.

35 N. Rivera, I. Kaminer, B. Zhen, J. D. Joannopoulos and M. Soljačić, Shrinking light to allow forbidden transitions on the atomic scale, *Science*, 2016, **353**, 263.

36 E. M. Lifshitz, The theory of molecular attractive forces between solids, *JETP USSR*, 1954, **29**, 94[English translation: Soviet Physics 1956, **2**, 73].

37 E. M. Lifshitz and L. P. Pitaevskii, *Landau and Lifshitz Course of Theoretical Physics, Vol.9: Statistical Physics - Part 2*, Pergamon Press, 1980.

38 H. B. G. Casimir, On the attraction between two perfectly conducting plates, *Proc. Ned. Akad. Wet.*, 1948, **51**, 793.
39 X. He, W. Gao, L. Xie, B. Li, Q. Zhang, S. Lei, J. M. Robinson, E. H. Hároz, S. K. Doorn, W. Wang, R. Vajtai, P. M. Ajayan, W. W. Adams, R. H. Hauge and J. Kono, Wafer-scale monodomain films of spontaneously aligned single-walled carbon nanotubes, *Nat. Nanotechnol.*, 2016, **11**, 633.
40 L. Liu, J. Han, L. Xu, J. Zhou, C. Zhao, S. Ding, H. Shi, M. Xiao, L. Ding, Z. Ma, C. Jin, Z. Zhang and L.-M. Peng, Aligned, high-density semiconducting carbon nanotube arrays for high-performance electronics, *Science*, 2020, **368**, 850.
41 N. Komatsu, M. Nakamura, S. Ghosh, D. Kim, H. Chen, A. Katagiri, Y. Yomogida, W. Gao, K. Yanagi and J. Kono, Groove-assisted global spontaneous alignment of carbon nanotubes in vacuum filtration, *Nano Lett.*, 2020, **20**, 2332.
42 G. J. Brady, A. J. Way, N. S. Safron, H. T. Evensen, P. Gopalan and M. S. Arnold, Quasi-ballistic carbon nanotube array transistors with current density exceeding Si and GaAs, *Sci. Adv.*, 2016, **2**, e1601240.
43 P.-H. Ho, D. B. Farmer, G. S. Tulevski, S.-J. Han, D. M. Bishop, L. M. Gignac, J. Bucchignano, P. Avouris and A. L. Falk, Intrinsically ultrastrong plasmon-exciton interactions in crystallized films of carbon nanotubes, *Proc. Natl. Acad. Sci. U. S. A.*, 2018, **115**, 12662.
44 J. A. Roberts, S.-J. Yu, P.-H. Ho, S. Schöche, A. L. Falk and J. A. Fan, Tunable hyperbolic metamaterials based on self-assembled carbon nanotubes, *Nano Lett.*, 2019, **19**, 3131.
45 M. E. Green, D. A. Bas, H.-Y. Yao, J. J. Gengler, R. J. Headrick, T. C. Back, A. M. Urbas, M. Pasquali, J. Kono and T.-H. Her, Bright and ultrafast photoelectron emission from aligned single-wall carbon nanotubes through multiphoton exciton resonance, *Nano Lett.*, 2019, **19**, 158.
46 W. Gao, C. F. Doiron, X. Li, J. Kono and G. V. Naik, Macroscopically aligned carbon nanotubes as a refractory platform for hyperbolic thermal emitters, *ACS Photonics*, 2019, **6**, 1602.
47 J. A. Roberts, P.-H. Ho, S.-J. Yu, X. Wu, Y. Luo, W. L. Wilson, A. L. Falk and J. A. Fan, Multiple tunable hyperbolic resonances in broadband infrared carbon-nanotube metamaterials, *Phys. Rev. Appl.*, 2020, **14**, 044006.
48 J. A. Roberts, P.-H. Ho, S.-J. Yu and J. A. Fan, Electrically driven hyperbolic nanophotonic resonators as high speed, spectrally selective thermal radiators, *Nano Lett.*, 2022, **22**, 5832.
49 S. Zhu, W. Li, S. Yu, N. Komatsu, A. Baydin, F. Wang, F. Sun, C. Wang, W. Chen, C. S. Tan, H. Liang, Y. Yomogida, K. Yanagi, J. Kono and Q. J. Wang, Extreme polarization anisotropy in resonant third-harmonic generation from aligned carbon nanotube films, *Adv. Mater.*, 2023, 2304082, DOI: **10.1002/adma.202304082**.
50 C. Kittel, *Introduction to Solid State Physics*, John Wiley & Sons, 8th edn, 2005.
51 P.-O. Chapuis, S. Volz, C. Henkel, K. Joulain and J.-J. Greffet, Effects of spatial dispersion in near-field radiative heat transfer between two parallel metallic surfaces, *Phys. Rev. B: Condens. Matter Mater. Phys.*, 2008, **77**, 035431.
52 D.-N. Le, P. Rodriguez-Lopez and L. M. Woods, Dispersive interactions between standard and Dirac materials and the role of dimensionality, *J. Phys. Mater.*, 2022, **5**, 034001.
53 M. Sadhukhan and A. Tkatchenko, Long-range repulsion between spatially confined van der Waals dimers, *Phys. Rev. Lett.*, 2017, **118**, 210402.
54 P. S. Venkataram, J. Hermann, A. Tkatchenko and A. W. Rodriguez, Unifying microscopic and continuum treatments of van der Waals and Casimir interactions, *Phys. Rev. Lett.*, 2017, **118**, 266802.
55 M. Stöhr, M. Sadhukhan, Y. S. Al-Hamdani, J. Hermann and A. Tkatchenko, Coulomb interactions between dipolar quantum fluctuations in van der Waals bound molecules and materials, *Nat. Commun.*, 2021, **12**, 137.
56 A. Benassi and C. Calandra, Vacuum fluctuation forces between ultra-thin films, *EPL*, 2008, **82**, 61002.